Optical properties of polycrystalline metallic films

Juan Sotelo*
Department of Applied Physics, University of Technology, Sydney, P.O. Box 123, Broadway NSW 2007, Australia

Jesper Ederth† and Gunnar Niklasson‡
Department of Materials Science, Division of Solid State Physics, University of Uppsala, The Angstrom Laboratory, SE-75121 Uppsala, Sweden

(Received 6 December 2002; published 20 May 2003)

We extend the Mayadas and Shatkes's approach [Phys. Rev. B **1**, 1382 (1970)] to study the optical properties of polycrystalline metal thick films in the visible and far infrared range of the spectrum. We show that in this range grain boundary scattering can account for the experimentally observed lowering of the film reflectivity as the mean size of its constituent grains decreases.

DOI: 10.1103/PhysRevB.67.195106 PACS number(s): 78.20.−e, 72.15.−v, 61.72.Mm

I. INTRODUCTION

The optical properties of metal films can be studied in terms of the optical conductivity which is associated with a transverse electron current density in the film. For isotropic materials, at sufficiently long wavelengths, in the infrared, the (transverse) optical conductivity converges to the ordinary (longitudinal) electrical conductivity. Electron transport properties of metal films taking account of grain boundaries have been studied over the years by several authors, using a variety of methods including the Boltzmann transport equation (and related approaches),[1–7] the transfer matrix in a one-dimensional (1D) quantum mechanical setting,[8] the energy loss concept,[9–11] and the superposition method.[12] Knowledge of the effect of grain boundaries in the electronic transport in these films may be used to obtain information on the microgeometry of the film,[10] analyze the transport properties of nonequilibrium electrons[13] and surface plasmons,[14] to name just a few applications.

Mayadas and Shatzkes (MS)[1,2] have calculated the total dc resistivity of a thin metal film using a model which accounts for electron scattering due to grain boundaries, the film boundaries and a homogeneous background. They used a semiclassical approach based on the Boltzmann transport equation, complemented by an independent determination of a collision term associated to grain boundaries. The background scattering is accounted for through a relaxation time, which is added to the contribution of grain boundary scattering. Admittedly, this assumption may be doubted because it is just another way to write Mathiessen's rule which is known to be violated in such a case.[15] Still, the assumption has been proven to hold, for instance, when the mean film grain size D is larger than the mean free path of the homogeneous background λ_∞,[12] and has even been pushed a little further to deal with some cases where $D \lesssim \lambda_\infty$.[12] Thus, the boundary of its applicability is not clearly defined. In spite of the model's shortcomings, its simplicity makes it appealing and useful as a first approximation when interpreting experimental data on electronic transport.[13,16,17] It would thus seem desirable to extend the model to be able to gain some insight into the optical properties of the films as well.

In this paper we extend the Mayadas and Shatzkes's electrical-resistivity model for polycrystalline films[2] to study grain boundary effects on optical properties of thick polycrystalline metallic films in the range of the spectrum spanning from the visible to the far infrared. This is done using the surface impedance approach to the reflectivity of a film by Kliewer and Fuchs.[18] We give explicit expressions for the dielectric function and surface impedance of the film in terms of the reflectance of the grain boundaries. Through this phenomenological parameter we analyze the effect of grain boundaries on the reflectance of the film. We also present results of experimental reflectance measurements that we have carried out in the range from the visible to the far infrared of the spectrum for gold films with grain mean-size between 15 and 45 nm, and compare those results with the computed reflectivity from our model. In the computations we use measured optical constants of single crystal gold, and model the optical properties of a polycrystal by introducing the effect of grain boundary scattering.

We begin by explicitly deriving the nonlocal optical conductivity of a polycrystal film for normal incident electromagnetic fields. We do this by solving a linearized Boltzmann transport equation for spatial and temporal dependent fields, for the 2D version of the Mayadas and Shatzkes model of a polycrystal. The solution of the equation is given in a form that allows us to estimate the contributions to the conductivity due to spatial dispersion and grain boundaries, which can then be used to assess the magnitude of their effects in the reflectivity and absorption properties of the films. The reflectivity and absorption are computed using the surface impedance formulation of the reflectivity of a film by Kliewer and Fuchs.[18] Using gold as an example, we show that by using the grain-boundary reflectance as the only adjustable parameter of our model, the calculated reflectivity of films with grain mean size in the range 15–45 nm is in good agreement with our experimental reflectivity measurements in most of the wavelength range of our study.

The plan of this paper is as follows. In Sec. II we present an extended Mayadas and Shatzkes's model based on the surface impedance concept to study the optical properties of thick polycrystalline films. In Sec. III we present the experimental procedure to obtain the reflectivity data of the films. The analysis and discussion of our results are given in Sec. IV, followed by the conclusions in Sec. V.

 ©2003 The American Physical Society

II. THE FILM MODEL AND COMPUTATIONAL PROCEDURE

Our model of a polycrystalline film is that proposed by Mayadas and Shatzkes[2] in their study of the effect of grain boundaries on the dc conductivity of thin polycrystalline films. In this model the grains in the film are considered to have columnar shape, extending upright from the bottom to the top surface of the film, and to be laterally bounded by perpendicular planes. These planes are represented by two uncorrelated sets of randomly located parallel planar potentials, which are short ranged and smooth so that only specular reflection is produced by planes that are parallel to an applied external field. Using this model we will first determine the film's optical conductivity taking account of the resistivity arising from two types of scattering mechanisms for the electrons, namely, specular scattering from sets of partially reflecting planar grain boundaries, together with isotropic background scattering produced by phonons and point defects.[2] Having determined the optical conductivity, we will next find the film's dielectric function, which we use to compute the film's surface impedance. In turn, we use this surface impedance to describe the optical properties of the film.

A. Optical conductivity

In order to find the optical conductivity of the film, we follow Kliewer and Fuchs (KF) (Ref. 18) and solve a linearized Boltzmann transport equation for time and space dependent fields, explicitly considering scattering due to short ranged grain-boundary potentials of the type described by Mayadas and Shatzkes (MS).[2] The Boltzmann transport equation is solved under the following assumptions which were introduced by Reuter and Sondheimer (RS),[19] MS,[2] and KF.[18] (RS1) Magnetic effects are dropped at the outset. (RS2) The film's linear dimensions L_x, L_y, and L_z are considered much greater than the penetration depth of the field, so that the film may be considered to have plane surfaces of infinite extent and essentially infinite thickness. (RS3) The electron states of the pure single crystal are taken as those corresponding to the free-electron hamiltonian, these states form an almost continuous set because of the large film volume $v=L_xL_yL_z$. (RS4) the conduction phenomena in the crystal is described in terms of a single parabolic band $\epsilon_{\mathbf{k}}=(\hbar^2/2m^*)\mathbf{k}^2$, where m^* is the effective mass of the electron, (RS5) the scattering at the film surface is specular. (MS1) Grain boundaries (plane potentials) are represented by δ-function potentials of strengths weak enough to allow the use of the Born approximation to calculate the electron transition rate for each of the arrays of parallel planes. (MS2) The scattering from phonons and point defects are accounted for by a relaxation time τ. (KF1) The wave vector k is small compared to the Fermi wave vector k_F and the frequency w is small compared to the Fermi frequency $\epsilon_F/\hbar$.

For definiteness we take the polycrystalline metallic film to fill the half-space $z\geqslant 0$, with its two uncorrelated sets of plane potentials taken to be orthogonal to the x and y axes, respectively. If we denote by ν either x or y, we have that the planes orthogonal to the ν axis are located at points $\{\nu_i, i=1,\ldots,N_\nu\}$ distributed according to a Gaussian $g_\nu(D_\nu,s_\nu)$ of mean D_ν and standard deviation s_ν.[2] Moreover, the action of the plane at ν_n is represented by a short range potential $S_\nu\delta(\nu-\nu_n)$ of strength S_ν.[2]

In what follows, we will only consider the case of an exciting electromagnetic wave of frequency w impinging normally on the film surface and polarized in the ν direction. Hence, all fields and currents in the film are assumed to have spatial and temporal dependence of the form $F(z,t)=F_\nu(z)\exp\{-iwt\}$, e.g., $E(z,t)=E_\nu(z)\exp\{-iwt\}$.

Let us denote by $g_{\mathbf{k}}(z,t)=f_{\mathbf{k}}(z,t)-f^0_{\mathbf{k}}$, the small deviation of the electron distribution function $f_{\mathbf{k}}(z,t)$ from its equilibrium value $f^0_{\mathbf{k}}$. As for the fields and currents we expect $f_{\mathbf{k}}$, and so $g_{\mathbf{k}}$, to have the same frequency dependance as the external field and to depend on position only through the distance z into the metal. The Boltzmann equation for our problem can then be written as

$$ev_{\mathbf{k},\nu}E\partial_{\epsilon_{\mathbf{k}}}f^0_{\mathbf{k}}=\frac{g_{\mathbf{k}}}{\tau}+\int P(\mathbf{k},\mathbf{k}')(g_{\mathbf{k}}-g_{\mathbf{k}'})d\mathbf{k}' + v_{\mathbf{k},z}\partial_z g_{\mathbf{k}}+\partial_t g_{\mathbf{k}}, \tag{1}$$

where $P(\mathbf{k},\mathbf{k}')$ is the transition probability for an electron in state $\mathbf{k}$ to be scattered to the state $\mathbf{k}'$ by the planes, $\epsilon_{\mathbf{k}}$ and $\mathbf{v}_{\mathbf{k}}$ are the energy and velocity, respectively, of an electron in state $\mathbf{k}$, and e is the magnitude of the electron charge.

Taking Fourier transform on both sides of this equation we get

$$ev_{\mathbf{k},\nu}\mathcal{E}\partial_{\epsilon_{\mathbf{k}}}f^0_{\mathbf{k}}=\frac{\mathcal{G}_{\mathbf{k}}}{\tau}+\int P(\mathbf{k},\mathbf{k}')(\mathcal{G}_{\mathbf{k}}-\mathcal{G}_{\mathbf{k}'})d\mathbf{k}'+iqv_{\mathbf{k},z}\mathcal{G}_{\mathbf{k}} - iw\mathcal{G}_{\mathbf{k}}, \tag{2}$$

where $\mathcal{G}_{\mathbf{k}}(q,w)$ and $\mathcal{E}(q,w)$ denote the Fourier transform of $g_{\mathbf{k}}(z,t)$ and $E(z,t)$, respectively.

To compute the transition probability $P(\mathbf{k},\mathbf{k}')$, $\mathbf{k}\neq\mathbf{k}'$, we proceed as in Ref. 2; an alternative procedure is given in Ref. 10 where use is made of the pair correlation function. Writing the grain boundary potential $V(\mathbf{r})$ as in Ref. 10,

$$V(\mathbf{r})=\sum_{\nu\in\{x,y\}}\sum_{n_\nu}S_\nu\delta(\nu-\nu_{n_\nu}), \tag{3}$$

the Born approximation yields

$$P(\mathbf{k},\mathbf{k}')=\frac{2\pi}{\hbar}\delta(\epsilon_{\mathbf{k}}-\epsilon_{\mathbf{k}'})\frac{v}{(2\pi)^3}\langle\langle|\langle\mathbf{k}|V|\mathbf{k}'\rangle|^2\rangle\rangle_{\mathfrak{g}} = \sum_{\nu\in\{x,y\}}F_\nu(|k_\nu|)\,\delta(k_\nu+k'_\nu)\,\delta(\mathbf{k}^\perp_\nu-\mathbf{k}'^\perp_\nu), \tag{4}$$

where $\langle\langle\cdots\rangle\rangle_{\mathfrak{g}}$ denotes the average over the distribution $\mathfrak{g}_x(D_x,s_x)\mathfrak{g}_y(D_y,s_y)$, $\mathbf{k}^\perp_\nu$ is the component of $\mathbf{k}$ transversal to the ν axis, and[2]

$$F_\nu(u)=\frac{\alpha_\nu}{2\tau}\frac{k_F}{u}h_\nu(u),\quad u>0, \tag{5}$$

$$\alpha_\nu = \frac{l_\infty}{D_\nu}\frac{R_\nu}{1-R_\nu}, \tag{6}$$

$$h_\nu(u) = \frac{1-\exp(-4u^2 s_\nu^2)}{1+\exp(-4u^2 s_\nu^2)-2\exp(-2u^2 s_\nu^2)\cos(2uD_\nu)}. \tag{7}$$

Here k_F denotes the magnitude of the Fermi wave vector, R_ν is the reflection coefficient from a single barrier in the ν direction, and l_∞ is the background mean free path.

With $P(\mathbf{k},\mathbf{k}')$ known, we seek a solution to Eq. (2) of the form

$$\mathcal{G}_\mathbf{k}(q,w) = \Phi_\mathbf{k}(q,w) v_{\mathbf{k},\nu}\mathcal{E}(q,w), \tag{8}$$

with $\Phi_\mathbf{k}$ satisfying

$$\Phi_{\{-k_x,k_y,k_z\}} = \Phi_{\{k_x,k_y,k_z\}}, \tag{9}$$

$$\Phi_{\{k_x,-k_y,k_z\}} = \Phi_{\{k_x,k_y,k_z\}}. \tag{10}$$

Replacing Eq. (8) into Eq. (2) gives

$$ev_{\mathbf{k},\nu}\partial_{\epsilon_\mathbf{k}} f^0_\mathbf{k} = \Phi_\mathbf{k} v_{\mathbf{k},\nu}[\tau^{-1} - i(w - v_{\mathbf{k},z}q)] + \int P(\mathbf{k},\mathbf{k}')(\Phi_\mathbf{k} v_{\mathbf{k},\nu} - \Phi_{\mathbf{k}'} v_{\mathbf{k}',\nu})d\mathbf{k}'. \tag{11}$$

The integral term can be evaluated using Eqs. (4), (9), and (10), we find

$$2F_\nu(|k_\nu|)\Phi_\mathbf{k} v_{\mathbf{k},\nu}. \tag{12}$$

Substituting this expression into Eq. (11), solving the latter for $\Phi_\mathbf{k}$ and inserting the result into Eq. (8) yields

$$\mathcal{G}_\mathbf{k}(q,w) = \frac{ev_{\mathbf{k},\nu}\partial_{\epsilon_\mathbf{k}} f^0_\mathbf{k}}{\tau_\nu^{-1} - i(w - v_{\mathbf{k},z}q)}\mathcal{E}(q,w), \tag{13}$$

$$\frac{1}{\tau_\nu} = \frac{1}{\tau} + 2F_\nu(|k_\nu|). \tag{14}$$

From the relations

$$\mathcal{J}_\nu(q,w) = \mathcal{E}(q,w)\sigma^{\mathrm{FC}}_{\nu\nu}(q,w) = -\frac{e}{4\pi^3}\int v_{\mathbf{k},\nu}\mathcal{G}_\mathbf{k}(q,w)d\mathbf{k}, \tag{15}$$

where $\mathcal{J}_\nu(q,w)$ is the Fourier transform of the current density $J_\nu(z,t)$, we obtain the tensor component $\sigma^{\mathrm{FC}}_{\nu\nu}(q,w)$ of the dynamical conductivity[9] of the free carriers (FC) in the presence of both grain boundary and background scattering

$$\sigma^{\mathrm{FC}}_{\nu\nu}(q,w) = \frac{e^2}{4\pi^3\hbar}\int \frac{v_{\mathbf{k},\nu}v_{\mathbf{k},\nu}}{\tau_\nu^{-1} - i(w - v_{\mathbf{k},z}q)}\frac{dS_F}{|\mathbf{v}_\mathbf{k}|} = \sigma^{\mathrm{D}}(w)\mathfrak{G}_\nu(q,w), \tag{16}$$

where the integral is over the Fermi sphere

$$\sigma^D(w) = \frac{\epsilon_0 w_p^2}{\tau^{-1} - iw}, \tag{17}$$

is the Drude-Sommerfeld conductivity of a single-crystal metal and

$$\mathfrak{G}_\nu(q,w) = \frac{3}{4\pi}\int \frac{\hat{k}^2_{F,\nu}d\Omega}{1+\alpha'_\nu h_\nu(|k_{F,\nu}|)|\hat{k}_{F,\nu}|^{-1} + l'_\infty \hat{k}_{F,z}q} \tag{18}$$

is a factor that takes into account grain boundary as well as spatial dispersion (nonlocality) effects. Here, $\hat{\mathbf{k}}_F$ denotes a unit vector along the direction of the Fermi wave vector $\mathbf{k}_F$, Ω denotes the solid angle and

$$\alpha'_\nu = \frac{\alpha_\nu}{1 - iw\tau}, \tag{19}$$

$$l'_\infty = \frac{l_\infty}{1 - iw\tau}. \tag{20}$$

For computational purposes, it is convenient to express the integral in Eq. (18) in polar coordinates (θ,ϕ), where θ is the polar angle from the ν axis (the polar axis) and ϕ is the azimuthal angle in the plane orthogonal to the ν axis. Writing $u = \cos\theta$ and choosing ϕ so that $\hat{k}_{F,\nu} = u$ and $\hat{k}_{F,z} = \sqrt{1-u^2}\sin\phi$ we find

$$\mathfrak{G}_\nu(q,w) = \frac{3}{2\pi}\int_0^{2\pi} d\phi \int_0^1 du \frac{u^3}{u + \alpha'_\nu + l'_\infty qu\sqrt{1-u^2}\sin\phi}. \tag{21}$$

The second term in the denominator of the above integrand gives the effective contribution of grain boundaries to the optical conductivity, the third, gives the contribution due to spatial dispersion. Furthermore, the integrand has been simplified by using $h_\nu(k_F u) = 1$, which is deduced from Eq. (7) as follows: $h_\nu(k_F u)$ depends on s_ν, the standard deviation of the distribution of particles' sizes, through terms of the form $\exp(-u^2 k_F^2 s_\nu^2)$. For typical values of s_ν found in experiments the relation $(k_F s_\nu)^2 \gg 1$ holds, it then follows from Eq. (7) that $h_\nu(k_F u)$ is bounded over the interval [0,1] and has the value 1 there, except in a very small neigborhood of $u = 0$, where in any case the whole integrand in Eq. (21) vanishes as $\mathcal{O}(u^3)$.

B. Dielectric function

We can now obtain the dielectric response of the film in the following way. First, in our system of reference the dielectric function of the film is a diagonal tensor. We write this tensor as

$$\boldsymbol{\epsilon} = \begin{pmatrix} \epsilon_{t,xx} & 0 & 0 \\ 0 & \epsilon_{t,yy} & 0 \\ 0 & 0 & \epsilon_l \end{pmatrix}, \tag{22}$$

where ϵ_t and ϵ_l are the transverse and longitudinal dielectric function, respectively. Since there are not grain boundaries

perpendicular to the z axis, ϵ_l is just the dielectric function of a single crystal metal. Also, ϵ_t and ϵ_l are given by

$$\epsilon_{t,\nu\nu}=1+\chi^{\mathrm{IB}}(w)+\chi^{\mathrm{FC}}_{\nu\nu}(q,w), \tag{23}$$

$$\epsilon_l=1+\chi^{\mathrm{IB}}(w)+\chi^{\mathrm{D}}(w). \tag{24}$$

Here, we have assumed that the susceptibility due to interband transitions χ^{IB} is the same in both cases. Moreover, the susceptibilities due to the free carriers $\chi^{\mathrm{FC}}_{\nu\nu}$ and χ^{D} are given by

$$\chi^{\mathrm{FC}}_{\nu\nu}(q,w)=i\frac{\sigma^{\mathrm{FC}}_{\nu\nu}(q,w)}{\epsilon_0 w}=\chi^{\mathrm{D}}(w)\mathfrak{G}_\nu(q,w), \tag{25}$$

$$\chi^{D}(w)=i\frac{\sigma^{D}(w)}{\epsilon_0 w}. \tag{26}$$

From Eqs. (23), (24), and (25) it follows that

$$\epsilon_{t,\nu\nu}(q,w)=\epsilon_l(w)+\chi^{D}(w)[\mathfrak{G}_\nu(q,w)-1]. \tag{27}$$

This equation together with Eq. (24) determines the dielectric response of the film.

C. Reflectance

The optical properties of the film can now be studied in terms of the film's surface impedance $Z_\nu(w)$. For light incident from vacuum normal to a sharp surface, and when the electrons are assumed to scatter specularly at the surface, the surface impedance, in units of $\sqrt{\mu_0/\epsilon_0}$, is given by[18]

$$Z_\nu(w)=\frac{1}{\pi}\left(\frac{2iw}{c}\right)\int_0^\infty \frac{dq}{(w/c)^2\epsilon_{t,\nu\nu}(q,w)-q^2}. \tag{28}$$

The reflectance and associated absorptance are then[18]

$$\mathcal{R}_\nu(w)=\left|\frac{Z_\nu(w)-1}{Z_\nu(w)+1}\right|^2, \tag{29}$$

$$A_\nu(w)=1-\mathcal{R}_\nu(w). \tag{30}$$

D. Some limiting expressions

We now give some limiting expressions derived from the above formalism. As we have said, the contribution of the spatial dispersion to the optical conductivity is given by the term $l'_\infty q u\sqrt{1-u^2}\sin\phi$ in Eq. (21). For a given frequency w, the strongest part of the Fourier spectrum is around wave number $q=\delta(w)^{-1}$,[20] where $\delta(w)$ is the skin penetration depth of the metal at frequency w, it follows that

$$|l'_\infty q|\approx\frac{l_\infty}{\delta(w)}[1+(w\tau)^2]^{-1/2}=\frac{\xi(w)}{\delta(w)}\left(1+\frac{1}{(w\tau)^2}\right)^{-1/2}, \tag{31}$$

where $\xi(w)=v_F/w$ represents the temporal dispersion of an electron at the Fermi surface.[20] The ratio of spatial dispersion to grain-boundary contribution in Eq. (21) is then $r=0.5l_\infty/[\delta(w)\alpha_\nu]$, where the factor 0.5 stands for the maximum value of $u\sqrt{1-u^2}|\sin\phi|$ in the region $(u,\phi)\in[0,1]\times[0,2\pi]$. The reciprocal of $|l'_\infty q|$ for single-crystal bulk gold and the ratio r for polycrystalline gold films with different grain mean size are plotted in Fig. 1 for wavelengths in the visible and near infrared range. The α_ν's for these films satisfy $1.5<\alpha_\nu<4.4$.

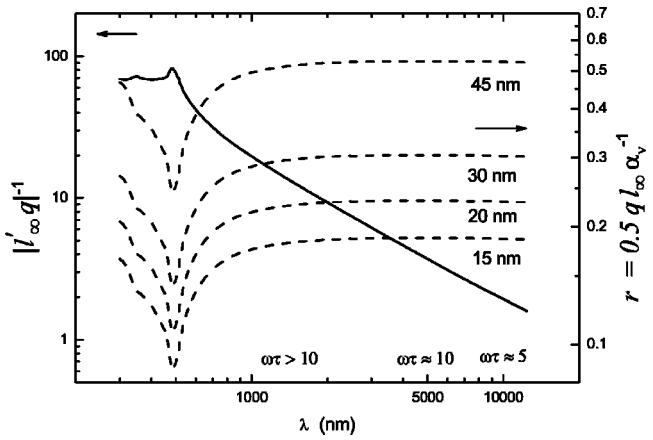

FIG. 1. Magnitude of the spatial dispersion and grain-boundary effects contributions to the optical conductivity of gold at $q\approx\delta(w)^{-1}$. Left axis: Reciprocal of the magnitude of the spatial dispersion term $l'_\infty q$. Right axis: Ratio, r, of spatial dispersion to grain-boundary contributions for polycrystalline films. The plots are labeled with the mean film grain size.

At short wavelengths $w\tau\gg1$; in this case, when $\delta(w)\gg\xi(w)$, the second relation of (31) shows that spatial dispersion is negligible, we may therefore take $q\approx0$. Provided that $r\ll1$, we can retain the term α'_ν in Eq. (21) and get

$$\mathfrak{G}_\nu(0,w)=1-\frac{3}{2}\alpha'_\nu+3\alpha'^2_\nu-3\alpha'^3_\nu\ln(1+\alpha'^{-1}_\nu). \tag{32}$$

Accordingly, Eq. (27) reduces to

$$\epsilon_{t,\nu\nu}(0,w)=\epsilon_l(w)-3\chi^{\mathrm{D}}(w)\alpha'_\nu\left(\frac{1}{2}-\alpha'_\nu+\alpha'^2_\nu\ln(1+\alpha'^{-1}_\nu)\right), \tag{33}$$

while $Z_\nu(w)$ [Eq. (28)] takes the simple form[18]

$$Z_\nu(w)=\epsilon_{t,\nu\nu}(0,w)^{-1/2}. \tag{34}$$

Substituting Eqs. (33) and (34) into Eq. (29) yields an analytic expression for the reflectance of the film which we shall henceforth refer to as the local reflectance.

On the other hand, at sufficiently long wavelengths $w\tau\ll1$ and $\delta(w)\gg l_\infty$,[20] hence, the first relation of Eq. (31) shows that spatial dispersion is again negligible ($q\approx0$). Since $r\ll1$ in this region, we can formally obtain $\mathfrak{G}_\nu(0,0)$ from Eq. (32), bearing in mind that $\alpha'_\nu\approx\alpha_\nu$ because $w\tau\ll1$, thus

$$\mathfrak{G}_\nu(0,0)=1-\frac{3}{2}\alpha_\nu+3\alpha_\nu^2-3\alpha_\nu^3\ln(1+\alpha_\nu^{-1}), \tag{35}$$

which corresponds to the ratio of the dc conductivity of a polycrystalline thick film to that of the bulk single crystal obtained by Mayadas and Shatzkes.[2]

The region between $\delta(w) \gg \xi(w)$ and $\delta(w) \gg l_\infty$ is the region of the anomalous skin effect,[20] where significant spatial dispersion occurs. In this case, we limit ourselves to numerically solve Eqs. (21), (27), and (28).

III. EXPERIMENTAL PROCEDURE

A. Experimental sample preparation

The samples used in this investigation were prepared by two different thin film deposition techniques: by the gas deposition method[21] and by resistive heating in vacuum. Concerning the gas deposition method, the evaporation from an ingot takes place in a lower chamber. The heating is provided by an induction coil of copper surrounding a carbon crucible containing Au of purity 99.999%. Nucleation and growth of nanoparticles takes place in the lower chamber. Particles are formed above the Au melt by condensation of the supersaturated Au vapor in He gas introduced from below the crucible. A transfer pipe is positioned centrally in the zone where particles are formed and ends in an upper chamber. Particles in an outer zone are removed by an exhaust pipe connected to the pump. Particle deposition took place onto a glass substrate mounted on a movable table in the upper chamber. Grain size was decreased by decreasing the temperature of the Au melt in the crucible. In the second fabrication procedure, resistive heating in vacuum, the chamber was kept at a pressure of $6-7\times10^{-6}$ mbar. Grain size was found to be related to the electric power used in the heating of the gold. Increased electric power gives larger grain size. Gold layers were produced with a thickness in the range 1–1.5 μm as measured using a Tencor Alpha Step 200 mechanical stylus.

B. Structural characterization

Structural characterization was performed on all samples using x-ray diffractometry employing a Siemens D5000 diffractometer. The grain mean diameter D was obtained by analyzing the full width at half maximum of the major peaks in the diffractogram using the method of Scherrer.[22] The D's for the four different samples considered in this paper were found to be 15, 20, 30, and 45 nm. The sample with D equal to 45 nm, was produced with the gas deposition method, and the other samples were produced by resistive heating in vacuum. Scanning electron microscopy was employed to verify the grain size obtained from x-ray diffractometry. It was found that the grain size obtained from the two independent characterization techniques were in good agreement, with a relative difference lower than 6%. Surface roughness was investigated on all samples using atomic force microscopy. Table I gives rms surface roughness data for each sample.

C. Optical properties

Spectral near normal reflectance was obtained in the wavelength range 0.3–50 μm. Ultraviolet, visible, and near-infrared reflectance 0.3–2.5 μm was measured on a Beckman spectrophotometer UV 5240 equipped with an integrating sphere. A plate of BaSO4 was used as reference material. Infrared reflectance was measured on a Perkin Elmer 983 infrared spectrophotometer in the wavelength range 2–50 μm. A gold film with grain mean size 45 nm was used as a reference. The reflectance data in the overlapping wavelength range, i.e., 2.0–2.5 μm, between the two different optical measurement ranges showed good agreement.

TABLE I. Data on grain size and corresponding r.m.s. surface roughness.

D (nm)	r.m.s. Surface roughness (nm)
15 ± 2	7.34
20 ± 3	5.98
30 ± 3	6.23
45 ± 3	8.49

IV. ANALYSIS OF DATA AND DISCUSSION OF RESULTS

We now use the model developed in Sec. II to analyze the reflectivity measurements of our polycrystal gold films in the visible and near infrared (VNIR) and in the far infrared (FIR). To simplify the calculations, we shall assume that the Gaussian distributions of grain sizes in the x and y axis have the same mean and standard deviation. In this context, the grain boundaries's reflectance will be simply denoted by R. In addition, we shall use the shorthand D-film to denote a film with a grain mean size of D nm. As said in Sec. III B our experimental data corresponds to reflectivity measurements for 15, 20, 30, and 45 films. For each one of these films, the reflectance data in the VNIR region is robustly fitted with the reflectance function (29), using the grain barriers's reflectance R as the only fitting parameter of the model. This gives the best value of R for each of the films. We then substitute these R's in Eq. (29) to compute the reflectance of the films in the FIR region. For each of the films, the above procedure is carried out, first, using the nonlocal dielectric function (27), and then using the local one (33).

The data fitting is done using the weighted orthogonal distance regression method implemented in ODRPACK, version 2.01.[23] The refractive index values for single crystal gold are obtained from Ref. 24. In addition we use the following values for the Drude parameters of gold at room temperature: $\hbar w_p = 8.98$ eV, $\hbar/\tau = 0.0237$ eV, $v_F/c = 0.00467$.

A. Visible and near infrared

Figure 2 presents experimental reflectance for all samples in the $400 < \lambda < 2250$ nm wavelength range. It is clearly shown that the near infrared reflectance is high for all samples. From the inset in Fig. 2 it is seen that the noise level is within 0.5% of the signal in the near infrared. The 45 film displays the highest reflectance in the whole wavelength range, and it is clearly observed that the near infrared reflectance decreases slightly with decreasing grain size. At $\lambda < 800$ nm absorption is prominent, and for the 45, 30, and 20

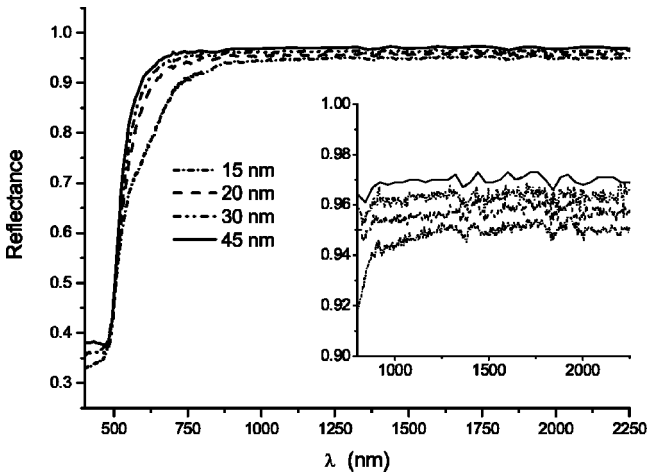

FIG. 2. Measured reflectivity for all the gold films. The inset shows a close up to the region 800–2250 nm.

films the reflectance displays a sharp steplike decrease at λ between 500–600 nm. This is due to interband transitions where electrons from the *d* bands are excited to the Fermi level. The 15 film, however, exhibit a different behavior with an extra absorption in the $550<\lambda<800$ nm range, which will be further discussed below.

For each of the films, its measured reflectivity and the model best fit to these measurements are shown in the plots of Fig. 3. The axes shown in the figure are those of the 45 films' plots. The plots corresponding to the other films are displayed vertically shifted downwards in steps of 0.1, and in order of decreasing grain mean size. In Table II we summarize the results of the fitting process for all the films. We see that the nonlocal and local computations give the same barrier reflectances. These barrier reflectances are higher than those previously reported for other materials using the MS model.[1,25] They are, however, well within the range 0.4–0.9 of reflectance values measured by scanning tunneling microscopy (STM) potentiometry on single grain boundaries in

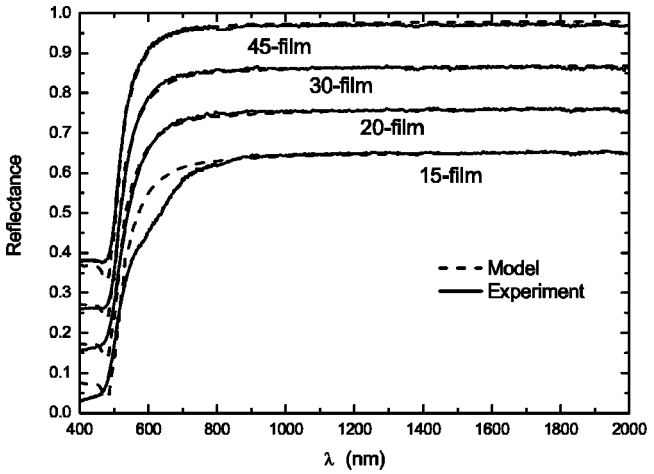

FIG. 3. Model best fit and measured reflectance for all the gold films. The plots of the 45 film are used as reference; the other plots have been vertically shifted downwards in steps of 0.1 and in order of decreasing grain mean size.

TABLE II. Barrier reflectance for several films with different grain mean size obtained from fits of the nonlocal and local models to the experimental data in the VNIR region.

D (nm)	R (nonlocal)	R (local)
15 ± 2	0.629 ± 0.05	0.629 ± 0.05
20 ± 3	0.645 ± 0.05	0.645 ± 0.05
30 ± 3	0.676 ± 0.05	0.675 ± 0.05
45 ± 3	0.643 ± 0.05	0.643 ± 0.05

Au,[26] and are lower than the value of 0.85 reported by Durkan and Wellan[16] obtained modeling a grain barrier as a missing row of atoms.

From the plots in Fig. 3 we can see that the model fits quite well the experimental data for the reflectance of the 20, 30, and 45 films over the whole wavelength range. For the 15 film, we also get good agreement with the experimental data in the region above 750 nm. Below this wavelength, however, it is clear from the plot that the model cannot account for the extra absorption present in the 550 to 750 nm range. Wooten[27] published reflectance data on unannealed Ag films displaying a shoulder at 340 nm, which was absent in annealed films. This shoulder was interpreted in terms of a surface plasmon excitation arising from the surface roughness. In our case, however, it is unlikely that the extra absorption of the 15 nm film is due to surface plasmon excitations caused by the surface roughness, since our films exhibit very similar rms values of the surface roughness; see Table I. Taneja and Ayyub[28] found a dip in the reflectance of nanocrystalline Ag films at $\lambda=350$ nm, which they assigned to surface plasmon resonance of the type generated in densely packed metal clusters of very small particles. It is conceivable that our 15 film exhibits a similar resonance due to (partial) confinement of electrons within the individual grains of the film. The width of the extra absorption peak is not easily obtained from Fig. 3. In order to obtain a quantitative estimate of the width, we performed a detailed ellipsometry investigation on our 15 film in the short wavelength region. It was found that the absorption coefficient displays a peak at $\lambda\approx600$ nm with a full width at half maximum (FWHM) of ≈0.26 eV. This is in good agreement with the FWHM of ≈0.24 eV, estimated from bulk optical constants by the expression of Kreibig[29] and setting the electron mean free path equal to the grain radius, e.g., 7.5 nm.

B. Far infrared (FIR)

Figures 4, 5, and 6 present experimental infrared reflectance for the 30, 20, and 15 films in the $3000\leqslant\lambda\leqslant12\,200$ nm range. In the figures, the reflectance has been normalized by dividing it with the reflectance of the 45 film. The level of infrared reflectance decreases with decreasing grain size, following the same trend as observed in the visible and near infrared wavelength range. The level of noise in the FIR, $\approx1.0\%$, is slightly higher than in the visible and near infrared, especially in the 2000–4000 nm range where it is fairly high.

Alongside the measured reflectivity of each of the films in the above figures, we also show the film's reflectance com-

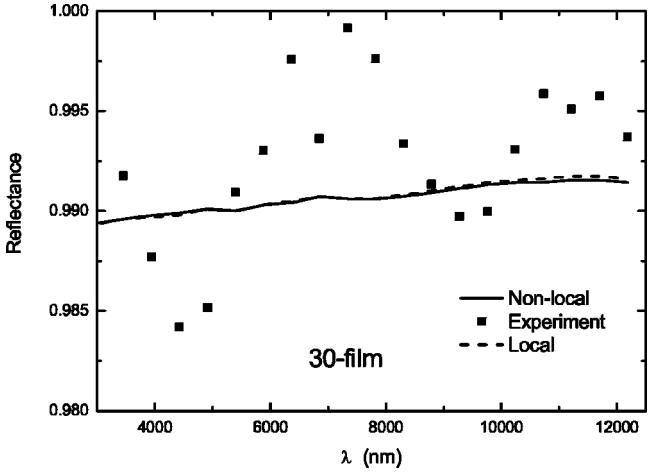

FIG. 4. Experimental and computed normalized reflectance of a gold film with grain size 30 nm.

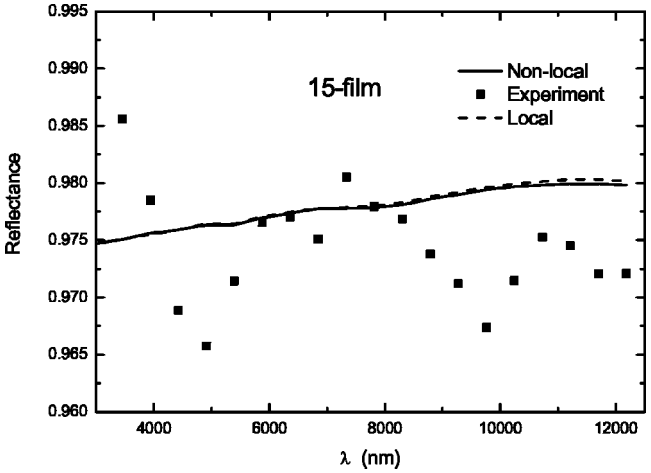

FIG. 6. Experimental and computed normalized reflectance of a gold film with grain size 15 nm.

puted using the local and nonlocal version of our model. As above, the reflectance has been normalized by the appropriate, local or nonlocal, computed reflectance of the 45 film. How far we can go in the FIR is limited by the extent of FIR data available in Ref. 24 for the optical constants of single-crystal gold, namely, $\lambda \leqslant 12\,500$ nm. We have, thus, limited our theoretical calculation to the wavelength range 3000–12 200 nm, where the lower cutoff wavelength is chosen so as to minimize the impact of the noisy region 2000–4000 nm in the comparison with experimental data, while still ensuring a range of wavelengths wide enough to include a sufficiently large sample of experimental points with which to test the theory.

From Figs. 4, 5, and 6 we observe that the classical reflectance (local) and the anomalous reflectance (nonlocal) cannot, at the scale of the figure, be distinguished from each other up to $\lambda \approx 9000$ nm, from there the classical reflectance becomes slightly higher than the anomalous one, the trend being the same for all the films. This is consistent with the analysis made at the end of Sec. II, for when $\lambda \gtrsim 9000$ nm, $w\tau \lesssim 6$ and we are in the weakly anomalous region, see Fig. 1, where the extra absorption causes a diminishing of the reflectivity. This effect should be more noticeable at wavelengths larger than 12 500 nm but shorter than wavelengths for which $\delta(w)/l_\infty \gg 1$; in this latter region spatial dispersion is negligible and the classical result holds once again. Furthermore, from Figs. 4 and 5 we conclude that the classical and anomalous calculations of the reflectance are in good agreement with the experimental data for the 30 and 20 films. Both calculations, however, overestimate the reflectance of the 15 film, see Fig 6. It is seen that the discrepancy we observe between computed and experimental reflectance increases as the grain size decreases, because, as suggested in Ref. 12, the assumption of additivity of inverse relaxation times becomes less accurate. This may also be due to our assumption of a columnar geometry for the grains of the film. In the region 3000–12 200 nm the skin depth is about 24 nm, thus for the 30 and 20 films the exciting field probes very weakly the actual layered structure of the film, and our columnar assumption is a good approximation to the microstructure of the film being probed in the reflectance measurement. For the 15 film, on the other hand, the exciting field does probe a few layers of grains in the film, this increases the film's resistivity leading to the measurement of a lower reflectance. In this case the assumption of a grain having columnar shape is only a rough approximation to the actual microstructure probed by the exciting field. We emphasize here that in the FIR region our model has no adjustable parameters; we use the barrier reflectance already determined in the calculations done in the VNIR region. This shows the robustness of the procedure used.

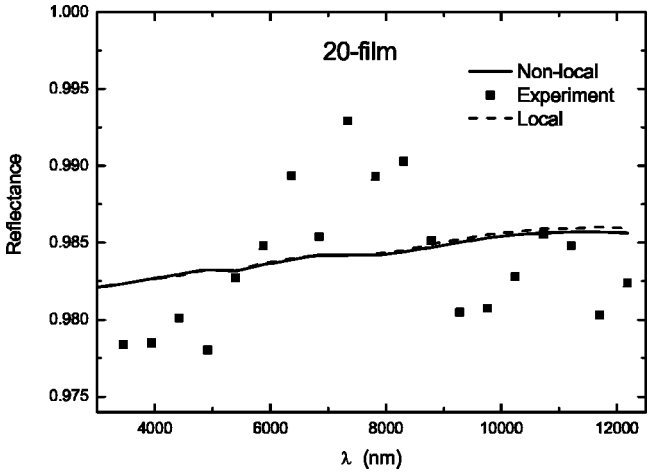

FIG. 5. Experimental and computed normalized reflectance of a gold film with grain size 20 nm.

V. CONCLUSIONS

We have carried out a study of the effect of grain boundaries on the optical properties of thick polycrystalline gold films in the wavelength range extending from the visible to the far infrared. Within the context of the Mayadas and Shatzkes approach, this effect has been expressed in terms of

a grain barrier reflectance. Using the semiclassical Boltzmann-transport equation approach we have found the dependence of the film's dielectric function on the grain barrier reflectance and expressed the reflectivity of the films through the films' surface impedance. We find that the experimental reflectivity measurement for gold films with mean grain size ranging from 15 to 45 nm, can be well explained by the above model, the agreement being best for films with mean grain size larger than 20 nm.

ACKNOWLEDGMENTS

J.S. acknowledges support from the Swedish National Science Research Council for his stay at the Angstrom Laboratory where part of this work was done. He also thanks Professor G.B. Smith for his warm hospitality at the Department of Applied Physics, University of Technology, Sydney, where this work was concluded. Anders Höel is acknowledged for performing the scanning electron microscopy.

*Permanent address: Departamento de Fisica, Informatica y Matematicas, Universidad Peruana Cayetano Heredia, Apartado Postal 4314 Lima, Peru. Email address: jsotelo@upch.edu.pe

†Electronic address: Jesper.Ederth@angstrom.uu.se

‡Electronic address: Gunnar.Niklasson@angstrom.uu.se

[1] A. F. Mayadas, M. Shatzkes, and J. F. Janak, Appl. Phys. Lett. **14**, 345 (1969).

[2] A. F. Mayadas and M. Shatzkes, Phys. Rev. B **1**, 1382 (1970).

[3] C. R. Pichard, C. R. Tellier, and A. J. Tosser, Thin Solid Films **62**, 189 (1979).

[4] C. R. Pichard, C. R. Tellier, and A. J. Tosser, Phys. Status Solidi B **99**, 353 (1980).

[5] F. Warkusz, Surf. Sci. **200**, 394 (1988).

[6] J. C. Dudek, Thin Solid Films **137**, 11 (1986).

[7] J. C. Dudek, Thin Solid Films **152**, 411 (1987).

[8] G. Reiss, J. Vancea, and H. Hoffman, Phys. Rev. Lett. **56**, 2100 (1986).

[9] E. Gerlach and P. Grosse, Adv. Solid State Phys. **17**, 157 (1977).

[10] E. Gerlach, Phys. Status Solidi B **187**, 477 (1995).

[11] E. Gerlach, Phys. Status Solidi B **203**, 107 (1997).

[12] A. Knäbchen, J. Phys.: Condens. Matter **3**, 6989 (1991).

[13] T. Juhasz, H. E. ElsayedAli, G. O. Smith, C. Suarez, and W. E. Bron, Phys. Rev. B **48**, 15 488 (1993).

[14] F. Moresco, M. Rocca, T. Hildebrand, and M. Henzler, Phys. Rev. Lett. **83**, 2238 (1999).

[15] R. Landauer, IBM J. Res. Dev. **1**, 223 (1957).

[16] C. Durkan and M. E. Welland, Phys. Rev. B **61**, 14 215 (2000).

[17] W. Steinhögl, G. Schindler, G. Steinlesberger, and M. Engelhardt, Phys. Rev. B **66**, 075414 (2002).

[18] K. L. Kliewer and R. Fuchs, Phys. Rev. **172**, 607 (1968).

[19] G. E. H. Reuter and E. H. Sondheimer, Proc. R. Soc. London, Ser. A **195**, 336 (1948).

[20] J. N. Hodgson, *Optical Absorption and Dispersion in Solids* (Chapman and Hall, London, 1970).

[21] J. Ederth, L. B. Kish, E. Olsson, and C. G. Granqvist, J. Appl. Phys. **88**, 6578 (2000).

[22] B. D. Cullity, *Elements of X-ray Diffraction* (Addison-Wesley, New York, 1956).

[23] P. T. Boggs, R. H. Byrd, J. E. Rogerse, and R. B. Schnabel (unpublished).

[24] J. H. Weaver, C. Krafka, D. W. Lynch, and E. E. Koch, *Optical Properties of Metals, Part II, Physics Data No. 18-2* (Fachinformationszentrum Energie, Physik, Mathematik, Karlsruhe, 1981).

[25] A. F. Mayadas, J. F. Janak, and A. Gangulee, J. Appl. Phys. **45**, 2780 (1974).

[26] M. A. Schneider, M. Wenderoth, A. J. Heinrich, M. A. Rosentreter, and R. G. Ulbrich, J. Electron. Mater. **26**, 383 (1997).

[27] F. Wooten, *Optical Properties of Solids* (Academic Press, New York, 1972).

[28] P. Taneja and P. Ayyub, Phys. Rev. B **65**, 245412 (2002).

[29] U. Kreibig, Appl. Phys. **10**, 255 (1976).